Neuron
Article

Anterior Regions of Monkey Parietal Cortex Process Visual 3D Shape

Jean-Baptiste Durand,[1,5] Koen Nelissen,[1,5] Olivier Joly,[1,5] Claire Wardak,[1] James T. Todd,[2] J. Farley Norman,[3] Peter Janssen,[1] Wim Vanduffel,[1,4] and Guy A. Orban[1,*]
[1] Lab Neuro- en Psychofysiologie, K.U. Leuven, Medical School, Campus Gasthuisberg, Herestraat 49, B-3000, Leuven, Belgium
[2] Department of Psychology, Ohio State University, 142 Townshend Hall, Columbus, OH 43210, USA
[3] Department of Psychology, Western Kentucky University, 1906 College Heights Boulevard, Bowling Green, KY 42101-1030, USA
[4] Athinoula A. Martinos Center for Biomedical Imaging, 13th Street, Charlestown, MA 02129, USA
[5] These authors contributed equally to this work.
*Correspondence: guy.orban@med.kuleuven.be
DOI 10.1016/j.neuron.2007.06.040

SUMMARY

The intraparietal cortex is involved in the control of visually guided actions, like reach-to-grasp movements, which require extracting the 3D shape and position of objects from 2D retinal images. Using fMRI in behaving monkeys, we investigated the role of the intraparietal cortex in processing stereoscopic information for recovering the depth structure and the position in depth of objects. We found that while several areas (CIP, LIP, and AIP on the lateral bank; PIP and MIP on the medial bank) are activated by stereoscopic stimuli, AIP and an adjoining portion of LIP are sensitive only to depth structure. Furthermore, only these two regions are sensitive to both the depth structure and the 2D shape of small objects. These results indicate that extracting 3D spatial information from stereo involves several intraparietal areas, among which AIP and anterior LIP are more specifically engaged in extracting the 3D shape of objects.

INTRODUCTION

Primates are unique in possessing both a versatile manipulative tool, the grasping hand (Napier, 1980), and an efficient system for guiding it in three-dimensional (3D) space, stereovision (Julesz, 1971; Wheatstone, 1838). Stereoscopic vision provides robust information about the shape and position of objects along the third dimension of visual space (i.e., their depth structure and position in depth), overcoming the loss of information inherent to the projection of a 3D visual scene onto 2D retinas (Howard and Rogers, 2002). Assessing the 3D shape of objects and their position in 3D space is important for selecting proper hand configurations for grasping them (Castiello, 2005; Jeannerod, 1986; Smeets and Brenner, 1999) and appropriate hand trajectories for reaching them (Jeannerod, 1981), respectively. Several intraparietal sulcus (IPS) regions are involved in the visual control of movements: the anterior intraparietal (AIP) area in grasping (Gallese et al., 1994; Sakata et al., 1995; Taira et al., 1990), the lateral intraparietal (LIP) area in saccades, and the medial intraparietal (MIP) area in reaching (Andersen and Buneo, 2002; Snyder et al., 1997). Yet, surprisingly little is known concerning how stereoscopic information is integrated into the control of goal-directed actions in the intraparietal cortex (Goodale and Milner, 1992; Ungerleider and Mishkin, 1982).

Stereovision allows the visual system to extract the depth structure of objects through the spatial integration of binocular disparity (Howard, 2002; Rogers and Cagenello, 1989). Combined with information regarding their 2D shape on the retina, depth structure provides a description of the 3D shape of objects, required for the control of grasping movements. Yet, it is unknown whether or not the anterior intraparietal (AIP) area gains access to 3D shape-related information. Neurons in AIP respond preferentially to some 3D objects and not to others (Murata et al., 2000), a finding which has been taken as evidence for 3D shape selectivity in this area. However, the use of objects differing along the three dimensions of space in this study does not preclude that AIP neurons are selective only for the 2D retinal shape of objects. Notably, such selectivity for 2D shapes has been found in the lateral intraparietal (LIP) area (Lehky and Sereno, 2007; Sereno and Maunsell, 1998), whose involvement in depth structure processing is unclear (Nakamura et al., 2001; Sereno et al., 2002; Vanduffel et al., 2002). In contrast, it has been established that neurons in the caudal intraparietal (CIP) area process the depth structure of planar surfaces (Tsutsui et al., 2005) from binocular disparity (Shikata et al., 1996; Taira et al., 2000) and/or monocular depth cues (Tsutsui et al., 2001, 2002). Nevertheless, many neurons in CIP prefer very large 3D surfaces and are weakly selective for the 2D shape of their bounding contours (Sakata et al., 1999; Shikata et al., 1996), questioning their involvement in 3D shape processing (Sakata et al., 1998, 2005). To date, neurons processing the shape of small visual objects along the three dimensions of space (i.e. selective both to their depth structure and to their 2D shape) have been found

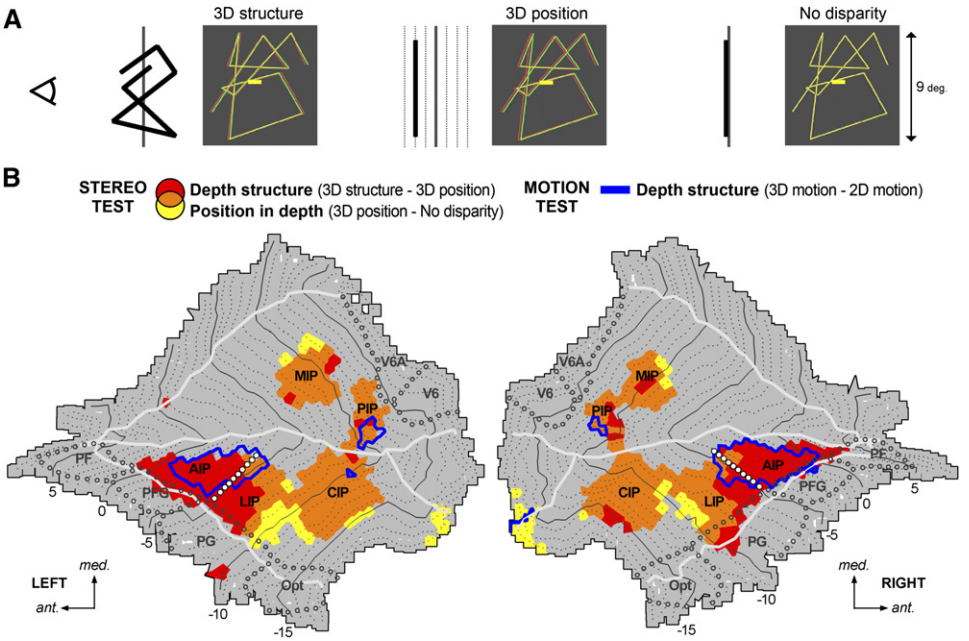

Figure 1. IPS Regions Processing Stereoscopic Information in Experiment 1

(A) Examples of stimuli for the three conditions (3D structure, 3D position, and No disparity) and schematic representation of the corresponding stereo percepts.

(B) Regions sensitive to structural and positional stereoscopic information are projected onto the flattened representations of left and right IPS, color coded in red and in yellow, respectively, with mixed sensitivity indicated in orange ($p < 10^{-5}$ uncorrected, masked by all stimulus conditions versus fixation baseline at $p < 10^{-3}$ uncorrected). Blue outlines delineate the regions sensitive to structural depth from motion (same statistical threshold). White dotted lines indicate the AIP/LIP borders derived from the saccade-related activity (same statistical threshold). Gray open symbols demarcate anatomically defined neighboring areas: Opt, PG, PFG, and PF on the inferior parietal lobule (Rozzi et al., 2006), and V6 and V6A on the parieto-occipital sulcus (Luppino et al., 2005).

only in a small region of the infero-temporal cortex (Janssen et al., 1999, 2000; Orban et al., 2006).

Besides its use in recovering the depth structure of 3D objects, stereovision also provides valuable information regarding the position of visual objects and their arrangement in 3D space. Such pieces of 3D spatial information are important for steering the hand toward an object (Jeannerod, 1981) while avoiding potential obstacles (Tresilian, 1998). Since the medial intraparietal (MIP) area controls arm-reaching movements (Buneo and Andersen, 2006; Snyder et al., 1997), its involvement in processing these positional and structural aspects of the 3D visual scene is likely but remains to be tested. Selectivity for the position in depth of stereo targets has been shown only in LIP (Genovesio and Ferraina, 2004; Gnadt and Mays, 1995), where such information is used for controlling eye movements in 3D space.

Here, we used functional imaging techniques with behaving monkeys (Vanduffel et al., 2001) to identify, in a first experiment, the intraparietal areas involved in processing structural and positional stereoscopic information. Stimuli were designed to engage regions processing the depth structure of either 3D objects or 3D arrangements of visual elements. Previous imaging studies have investigated 2D shape processing (Denys et al., 2004; Sawamura et al., 2005), stereoscopic depth processing (Tsao et al., 2003), and the extraction of depth structure from monocular cues (Sereno et al., 2002; Vanduffel et al., 2002), but these studies did not allow one to localize the regions involved in processing shape information along all three dimensions of space. We performed two additional experiments to identify the regions more specifically engaged in processing the 3D shape of visual objects. Since many of the objects we handle daily are typically bounded by small, curved surfaces yielding complex 2D shape outlines, these experiments were designed to identify the regions sensitive to the stereoscopic depth structure (curvature and orientation in depth) and the 2D shape of small and complex visual objects.

RESULTS

Experiment 1: Structural and Positional Depth Processing in the Intraparietal Cortex

The aims of the first experiment were to obtain an exhaustive picture of the intraparietal regions implicated in processing structural and positional stereoscopic information and also to compare the processing of depth structures from stereo and from motion. We used stimuli composed of connected random-line segments (Figures 1A and Figure S4A found in the Supplemental Data available with this article online), as used in previous motion experiments

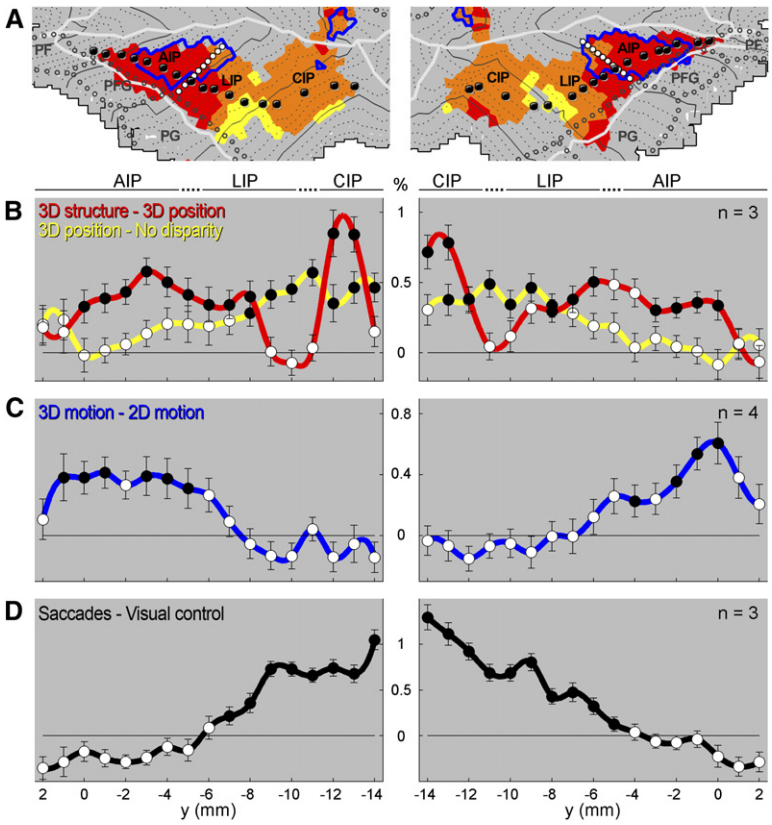

Figure 2. Path Activity Profiles for the Lateral Bank Activations in Experiment 1

(A) Paths running along postero-anterior axes on the IPS lateral banks, passing through CIP, LIP, and AIP. Black symbols indicate the flat map segments constituting the paths (one per coronal level; from −14 to +2 mm).

(B) MR signal change (± standard error of the mean) along the paths for the subtractions 3D structure – 3D position (red) and 3D position – No disparity (yellow). Filled symbols indicate the visually active segments for which MR signal change was significantly above zero (one-tailed t test), both for the group ($p < 0.001$) and for 2/3 of the individuals ($p < 0.01$). Note that, while results issued from path activity profiles and those given by SPM99 are very consistent with each other, slight differences can arise due to the use of unsmoothed data and additional statistical requirements (significance for 2/3 of the individuals) in the path activity profiles.

(C and D) Same as (B) for the subtraction 3D motion – 2D motion in the 3D motion test (C), and for the subtraction Saccades – Visual control in the Saccade test (D). (n, number of monkeys).

(Orban et al., 1999; Vanduffel et al., 2002). Such stimuli can be considered either as 3D objects (resembling partially unfolded paper clips) or as collections of line segments forming 3D structures. They contain both first- and second-order depth, defined by the spatial orientation of the segments and by their connections, respectively.

In the stereo test, sensitivity to depth structure was assessed by contrasting stimulus conditions in which binocular disparity specified 3D patterns of connected segments (3D structure; Figure 1A, left column) or 2D fronto-parallel patterns away from the fixation plane (3D position; Figure 1A, central column). Note that depth structure in such stereo stimuli can be recovered from orientation disparity and/or disparity gradients. We targeted sensitivity to position in depth (zero-order depth) by contrasting the condition 3D position with a no-disparity condition (Figure 1A, right column) in which equivalent stimuli were systematically displayed in the fixation plane. We scanned three animals while they performed a demanding high-acuity fixation task (Sawamura et al., 2005; Vanduffel et al., 2001). To assess sensitivity to depth structure from motion, we used monocular versions of the same stimuli. Motion specified either rotating 3D patterns of connected segments (3D motion) or 2D patterns translating horizontally in the fixation plane (2D motion).

Figure 1B presents, overlaid onto flattened representations of the left and right intraparietal sulcus (IPS; see Experimental Procedures), results of the group analysis (SPM99) for the stereo sensitivity to structural information (red), to positional information (yellow), and to both (orange). Several regions are stereosensitive, with mixed sensitivities to structural and positional information located mainly in the posterior half of the IPS (both lateral and medial banks). The posterior activation on the lateral bank corresponds to area CIP, where neurons have been shown to respond selectively to the 3D orientations and positions of rod stimuli (Sakata et al., 1998). It also closely matches the architectonically defined lateral occipital parietal (LOP) area (Lewis and Van Essen, 2000; Figure S1) and a region previously documented for its 2D shape sensitivity and named pIPS (Denys et al., 2004). The second activation on the lateral bank stretches from a location dorsal to CIP to a location close to the anterior tip of the IPS. It exhibits a heterogeneous pattern of depth sensitivity, with positional sensitivity in the back, structural sensitivity in the front, and an intermediate region of mixed sensitivity, which extends further ventrally. The white dotted lines in Figure 1B indicate the border between LIP and AIP. It was derived from the saccade-related activity (Baker et al., 2006; Gnadt and Andersen, 1988) obtained from an independent experiment (C. Wardak et al., 2005, Soc. Neurosci., abstract; see Experimental Procedures) showing that LIP, but not AIP, responded to saccadic eye movements (Figure 2). The location (y ∼−5 mm) of this border agrees with other studies (Luppino et al., 1999; Murata et al., 2000), and it reveals that AIP is sensitive

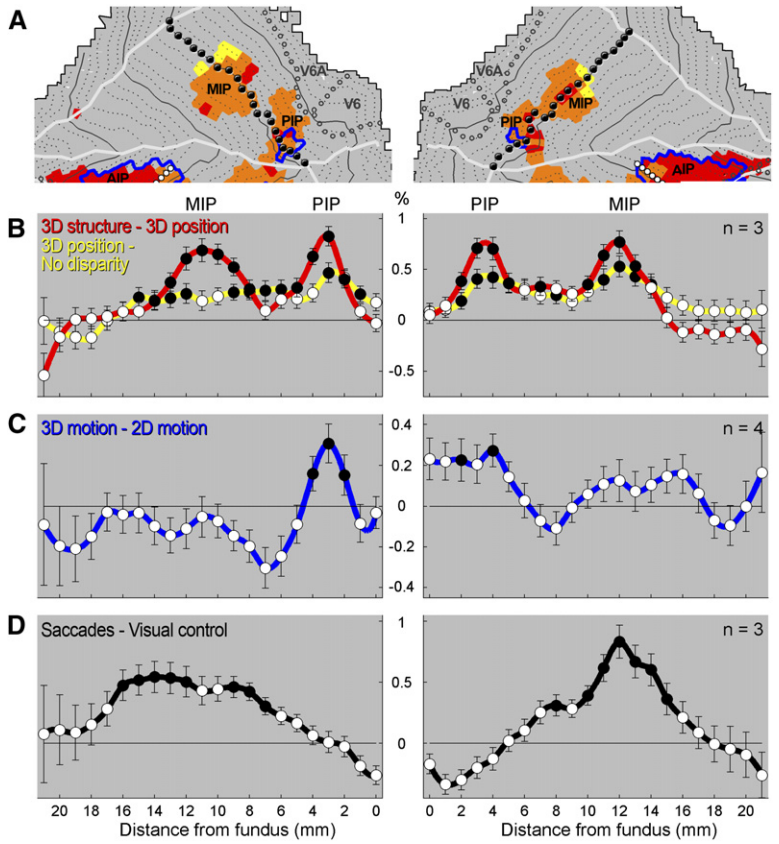

Figure 3. Path Activity Profiles for the Medial Bank Activations in Experiment 1

(A) Paths running along ventro-dorsal axes on the IPS medial banks, from the fundus to the medial lips, and passing through PIP and MIP. Black symbols represent the flat map segments constituting the paths (in adjoining coronal segments at −11 mm, from the fundus to PIP, and at −10 mm, from MIP to the medial lip).

(B–D) MR signal change (± SEM) along these paths for the subtractions 3D structure – 3D position (red) and 3D position – No disparity (yellow), in the first stereo experiment (B), for the subtraction 3D motion – 2D motion in the 3D motion test (C), and for the subtraction Saccades – Visual control in the Saccade test (D). Same conventions as Figure 2.

only to depth structure from stereo, while the heterogeneous pattern of depth sensitivity described above mainly belongs to LIP.

We drew paths passing through CIP, LIP, and AIP directly onto the flattened IPS representations (Figure 2A) and plotted the magnetic resonance (MR) signal change along these paths for contrasts of interest (Figures 2B–2D; see Experimental Procedures). Red and yellow "path activity profiles" in Figure 2B indicate, respectively, stereo sensitivity to structural (3D structure − 3D position) and positional (3D position – no disparity) information (the 0% level corresponds to an equal MR signal change in the two conditions). Filled symbols indicate data points (flat map segments) with significant sensitivity (i.e., significantly above the 0% difference level) and significant activation (compared to fixation) at the group level and for at least 2/3 of the individuals. These path activity profiles confirm the results drawn at the group level: CIP is sensitive to both structural and positional information while AIP is sensitive only to structural information. They also indicate that the heterogeneous stereodepth sensitivity in LIP emanates from opposing sensitivity gradients, with increasing sensitivity to structural information and decreasing sensitivity to positional information from its posterior to its anterior end. Note that enlarging the width of these paths (five segments instead of one at each coronal level) had little effect on the activity profiles (Figure S2), indicating that similar conclusions would have been drawn with slightly different paths.

On the medial bank, two posterior regions were sensitive to both structural and positional information from stereo (Figure 1B). Their location, anterior to areas V6/V6A (Luppino et al., 2005), correspond to MIP and to the anterior portion of the posterior intraparietal (PIP) area as defined by Lewis and Van Essen (2000). The MR signal change sampled along paths passing through MIP and PIP (Figure 3A) confirmed, at the group level and in individual subjects, the stereo sensitivity of these medial bank areas both for structural (Figure 3B, red curve) and positional (yellow curve) information. Once again, enlarging the width of these paths had little effect on the activity profiles (Figure S2). The presence of saccade-related activity in MIP (Figure 3D) is in line with a previous single cell study (Snyder et al., 2000). Note that despite their spatial proximity, PIP differs from MIP, and also from CIP (Figure 2D), by the absence of saccade-related activity.

Since a weak sensitivity to kinetic depth (Wallach and O'Connell, 1953) has been described in the monkey intraparietal cortex (Vanduffel et al., 2002), we assessed its involvement in processing depth structure from motion using monocular versions of the same stimuli. Sensitivity to depth structure from motion was assessed by contrasting 3D motion and 2D motion conditions. The same three monkeys as those used in the stereo test, plus an

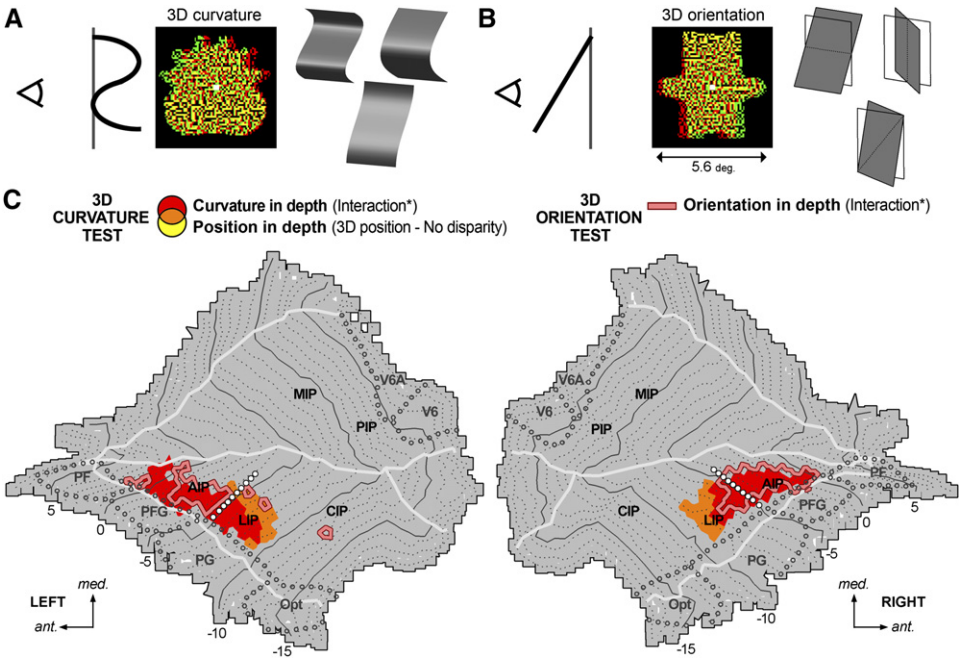

Figure 4. IPS Regions Sensitive to the Curvature and Orientation in Depth of Stereo Surfaces in Experiment 2

Examples of stimuli for the 3D curvature (A) and 3D orientation (B) conditions, and schematic representation of the corresponding stereo percepts. Several curvature and slant profiles specified by binocular disparity were used for testing 3D curvature and 3D orientation processing in interleaved runs. (C) Regions sensitive to curvatures in depth and positions in depth are projected onto the flattened representations of left and right IPS with the same conventions as Figure 1. Pink outlines delineate the regions sensitive to orientations in depth from stereo. (*sensitivity to structural depth, either curvature or orientation, was assessed by the interaction between disparity and depth order).

additional monkey included in a previous study (Vanduffel et al., 2002), were involved in this motion test. As shown in Figure 1B (blue outlines), only AIP (with possibly a slight extension into ventral LIP) and the ventral part of PIP were sensitive to structural information specified by motion. Plotting the MR signal change for the subtraction 3D motion – 2D motion along the same paths as those used for the stereo test confirmed the sensitivity of AIP (Figure 2C) and PIP (Figure 3C) to depth structure from motion at the group and at the individual-subject level (see also Figure S2 for confirmation with larger paths).

These results add to the evidence of a functional heterogeneity between neighboring areas PIP and MIP, with sensitivity to depth from motion found only in PIP (Figure 3C) and saccade-related activity only in MIP (Figure 3D). Importantly, while the depth structure of random lines specified by stereo activates a large intraparietal network, equivalent information defined by motion engages only a restricted network in the IPS.

Experiment 2: Depth Structure Processing for Stereo Surfaces in the Intraparietal Cortex

This second experiment was designed to identify the intraparietal regions most specifically engaged in processing the depth structure of small and relatively complex visual objects. We used stereo random-dot surfaces bounded by irregular 2D shape outlines (Figures 4A and 4B and Figure S4B), whose 3D structure is processed by neurons in the infero-temporal cortex (Janssen et al., 1999, 2000). In interleaved runs, we tested for differences in the sensitivity to curvature in depth (second-order depth; Figure 4A) and orientation in depth (first-order depth; Figure 4B). We scanned three monkeys (two of which were involved in the stereo and motion tests of the first experiment) in a 2 × 2 factorial design with four stimulus conditions (3D structure, 3D position, and their respective controls without disparity; see Experimental Procedures). We identified depth structure sensitivity, for either curvature or orientation in depth, by the interaction between disparity (disparity versus no disparity conditions) and depth order (structural versus positional conditions). Position in depth sensitivity was assessed by contrasting the 3D position condition and its control condition with no disparity.

As shown in Figure 4C for the group of three monkeys, sensitivity to the curvature in depth of these small stereo surfaces (red and orange) was restricted to AIP and an adjoining portion of LIP. Sensitivity to their orientation in depth (pink outlines) largely overlapped, although it extended slightly less into LIP. Sensitivity to structural and positional information from stereo (orange) was again found in LIP.

Using the same lateral paths (Figure 5A) as those in the first experiment (Figure 2A), we assessed the sensitivity to structural depth information, either curvature (Figure 5B) or orientation (Figure 5C) by plotting the MR signal change for the subtraction 3D curvature (or orientation) – 3D

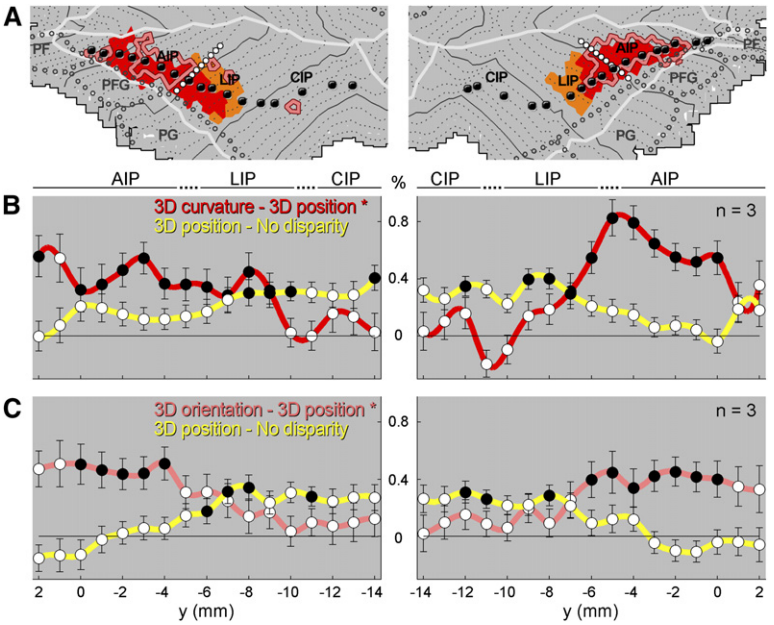

Figure 5. Path Activity Profiles for the Lateral Bank Activations in Experiment 2

(A) Same paths as Figure 2.

(B) MR signal change (± SEM) along the paths for the subtractions 3D curvature –3D position (*after subtraction of their respective No disparity control), in red, and 3D position – No disparity, in yellow, in the 3D curvature test.

(C) Same as (B) for the subtraction 3D orientation – 3D position, in pink, and 3D position – No disparity, in yellow, in the 3D orientation test. Same conventions as Figure 2.

position after subtracting their respective control lacking disparity. Sensitivity to positional information was derived from by the subtraction 3D position – no disparity. These path activity profiles confirmed, for the individual subjects as well, that AIP is sensitive both to the curvature in depth (Figure 5B, red curve) and to the orientation in depth (Figure 5C, pink curve) of these stereo surfaces, but not to their position in depth (Figures 5B and 5C, yellow curves). These path activity profiles also confirmed the presence of opposing sensitivity gradients for structural and positional information in LIP, as shown in the first experiment (Figure 2B).

Thus, although less extensive than in the first experiment, the stereo activations found in AIP and the adjoining part LIP presented similar features in the two experiments. However, in striking contrast, posterior parietal regions were only weakly (CIP) or not at all (MIP, PIP) engaged by these small stereo surfaces bounded by complex 2D outlines.

Experiment 3: 2D Shape Processing in the Intraparietal Cortex

After identifying the regions involved in processing the depth structure of small objects, we studied 2D shape sensitivity within the intraparietal cortex by complementing and reanalyzing a previous monkey imaging study (Denys et al., 2004) and performing an additional control experiment.

The same three monkeys as those used in the first experiment were involved in the experiment that replicated the protocol of Denys et al. (2004). Stimuli were grayscale images and line drawings of objects that were contrasted with spatially scrambled versions of the same stimuli (Figure 6A) to assess 2D shape sensitivity. Figure 6C presents the 2D shape-sensitive regions (pale and dark blue) obtained in the group analysis from the main effect of scrambling. In agreement with this previous study, we found two regions sensitive to 2D shapes on the lateral bank of the IPS. The posterior region, called pIPS in this previous study, closely matches the central and ventral parts of CIP, as defined in the first experiment. The anterior region includes both AIP and the anterior part of LIP, distinguished by the saccade-related activity (Figure 2D). Using the same lateral paths (Figure 7A) as those used in previous analyses (Figures 2 and 5), we plotted the difference in MR signal change for the subtraction intact – scrambled images (Figure 7B) for the grayscale images (circular symbols) and line drawings (square symbols) separately. Both profiles indicate that 2D shape sensitivity peaks within CIP and near the border between LIP and AIP.

The line drawing stimuli represent only impoverished versions of the grayscale stimuli, lacking the detailed shape-related information contained in the objects' surfaces and defined by their texture and/or luminance (Kourtzi and Kanwisher, 2000). To reveal the intraparietal regions sensitive to this additional information, we looked at the interaction between image type and scrambling. As indicated by the dark blue regions in Figure 6C, a significant interaction between image types and scrambling was found in the anterior, but not posterior, regions. Inspection of the activity profiles (Figure 7B) confirmed the preference for grayscale images in LIP and AIP (dark blue asterisks indicate significant difference between the curves for the group and at least 2/3 of the individuals). Thus, filling the surfaces of objects defined by their 2D shape outlines induces additional activation only in these anterior regions, indicating that they integrate information about contours and surfaces for representing visual objects.

Using smaller grayscale images of objects (size of 4.6° on average against 10° on average in the study of Denys

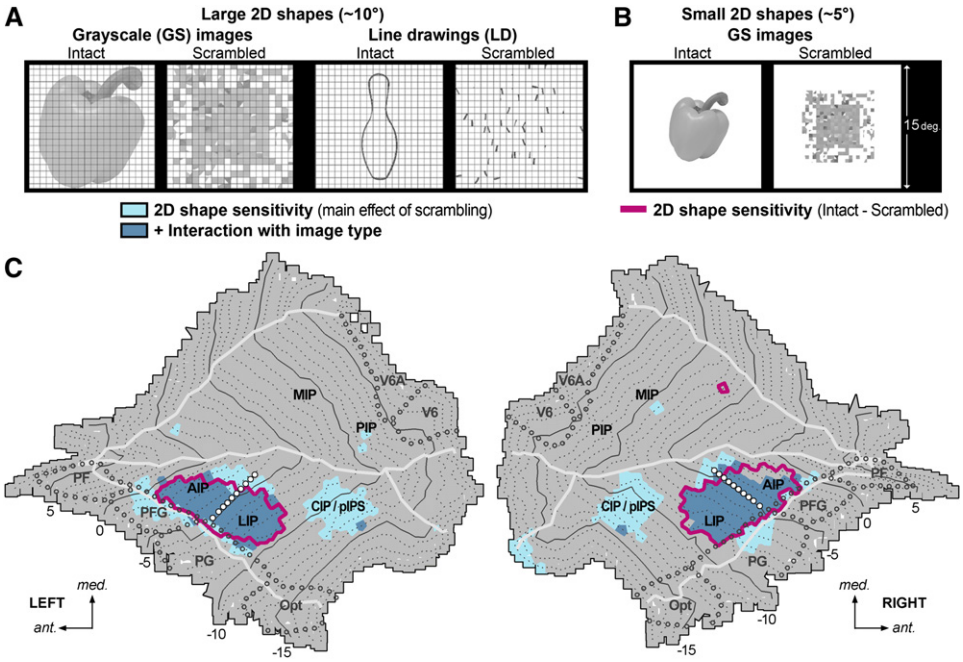

Figure 6. IPS Regions Sensitive to 2D Shapes in Experiment 3

(A) Examples of grayscale images and line drawings of objects, presented with their respective scrambled control (Denys et al., 2004; Kourtzi and Kanwisher, 2000).

(B) Example of a half-sized (from ~10° to ~5° on average) grayscale image and its scrambled version as used in the control experiment (overall size of the stimuli was identical: 15°).

(C) 2D shape-sensitive regions projected onto the flattened representations of left and right IPS. Blue regions, whether pale or dark, indicate a significant main effect of scrambling for large 2D shapes. Dark blue regions exhibit in addition a significant interaction between scrambling and image type in the test with large shapes. Magenta outlines delineate the 2D shape-sensitive regions for the half-sized grayscale images. Same conventions as Figure 1.

et al.), Sawamura et al. (2005) found only one region sensitive to 2D visual shapes, situated in the anterior portion of the IPS lateral bank. To assure that the discrepancy between these studies depended on stimulus size rather than on a difference between the sets of images, we performed a control experiment with a smaller version (50% scaling) of the grayscale stimuli (Figure 6B) used by Denys et al. (2004), adjusting the stimulus size to approximate those in the study of Sawamura et al. (2005). We scanned two of the three monkeys involved in the test with large 2D shapes. Magenta outlines in Figure 6C indicate the 2D shape-sensitive regions obtained by contrasting the intact and scrambled versions of these smaller grayscale images of objects. It can be seen that 2D shape sensitivity disappears in CIP but is still present within LIP and AIP. Path activity profiles for the intact – scrambled subtraction (Figure 7C) confirmed the sensitivity of LIP and AIP to small 2D shapes at the group level and in individual subjects. The interaction term between scrambling and size (2-way ANOVA) was significant in CIP, (Figure 7C; asterisks), indicating that CIP responds to large, but not small, 2D shapes. These activity profiles also indicate that 2D shape sensitivity peaks at the same location, near the AIP-LIP border, for large (Figure 7B; circular symbols) and small (Figure 7C) 2D shapes.

DISCUSSION

The first experiment revealed the involvement of several intraparietal areas in processing the arrangement in depth of connected random line segments: CIP, LIP and AIP, on the lateral bank and PIP and MIP on the medial bank. Such an extensive network underscores the importance of stereopsis for visually guided actions (Melmoth and Grant, 2006; Servos et al., 1992; Watt and Bradshaw, 2003) and contrasts with the restricted network (AIP and part of PIP) involved in kinetic depth extraction (Vanduffel et al., 2002). These parietal areas differed markedly regarding both the type of information and the type of stimuli they process. Posterior areas (CIP, PIP, and MIP) are sensitive to both structural and positional stereo information. In LIP, stereo-depth sensitivity is inhomogeneous, with opposing gradients of increasing sensitivity to depth structure and decreasing sensitivity to position in depth from its posterior to its anterior end. More anteriorly, AIP processes solely depth structure information specified either by stereo or motion. The second experiment revealed that, among these parietal areas, only AIP and the adjoining portion of LIP are clearly involved in processing the curvature and orientation in depth of small stereo surfaces bounded by complex 2D shape outlines. The third

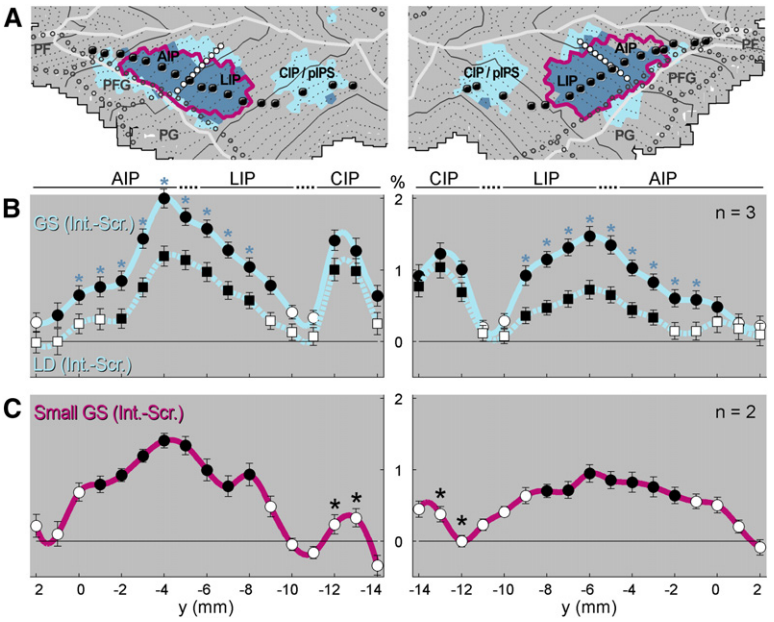

Figure 7. Path Activity Profiles for the Lateral Bank Activations in Experiment 3

(A) Same paths as Figure 2.

(B) MR signal change (± SEM) along the paths for the subtraction Intact – Scramble for the grayscale images (circles) and for the line drawings (squares) with large 2D shapes. Dark blue asterisks indicate significant difference (two-tailed t test) between these two subtractions, at the group level ($p < 0.001$) and for at least 2/3 of the individuals ($p < 0.01$).

(C) Same as (B) for the subtraction Intact – Scramble in the test with small grayscale shapes. Black asterisks indicate a significant interaction in the 2-way ANOVA with stimulus size and scrambling as factors ($p < 0.05$ at the group level and for the two individuals, Bonferroni correction for the number of tests). Same conventions as Figure 2.

experiment showed that LIP and AIP are also sensitive to 2D shapes, whether large or small, and integrate information about contours and surfaces. In contrast, CIP, found to correspond to the 2D shape-sensitive region named pIPS (Denys et al., 2004) but also to the architectonically defined area LOP (Lewis and Van Essen, 2000; see Figure S1), was recruited mainly for large 2D shapes, and responded chiefly to their contours. These results, drawn at the group level, were found bilaterally, and they were confirmed for at least 2/3 of the individuals with path activity profiles, ensuring their generality. The same three monkeys were involved in the first and third experiment, and two of these animals were also involved in the second experiment, making unlikely that our results are confounded by between-group heterogeneity.

Since the parietal cortex is involved in spatial attention (Colby and Goldberg, 1999; Goldberg et al., 2006), it is important to assess whether our results could be explained by the fact that certain stimulus conditions engage the observers' attention more strongly than others (for instance, 3D stimuli could capture attention more effectively than 2D stimuli and 2D stimuli more so than their scrambled counterparts). The attention-demanding high-acuity fixation task (Sawamura et al., 2005; Vanduffel et al., 2001) used in the first experiment entails a negative manipulation of spatial attention (drawing attention away from the stimuli) and is thus presumed to minimize or cancel any stimulus-driven attentional effect. Nevertheless, a broad stereo network was revealed in the intraparietal cortex by this first experiment, arguing against an explanation of our results based upon an attentional effect. Using a comparable task, Denys et al. (2004) reached a similar conclusion concerning 2D shape sensitivity in the IPS. Moreover, while an attentional explanation would predict rather homogeneous activation patterns reflecting the degree of attention captured by different stimulus types, we observed distinct differences in functional properties regarding depth and shape processing, between parietal areas, and even within LIP. In addition, our results are in agreement with the few single cell studies that addressed neuronal selectivity in these parietal areas regarding both depth and shape processing (see below). Differential eye movements across stimulus conditions is another possible confound, notably because binocular disparity is known to evoke fusional vergence eye movements (Boltz and Harwerth, 1979). However, eye movements were systematically monitored during scanning and quality of fixation across stimulus conditions was assessed (Table S1) so that this potential confound could be ruled out.

Our results show that AIP and an adjoining portion of LIP have a prominent role in processing the 3D shape of visual objects, since they are sensitive both to their depth structure and to their 2D shape. In AIP, neuronal selectivity to real 3D objects has been documented (Murata et al., 2000), but with objects differing along the three dimensions of space. Thus, whether this selectivity originated from the distinct depth structure and/or 2D optical projection of these objects could not be assessed directly. Since both sources of information are essential for recovering 3D shape features that can serve to control hand manipulation tasks (Fagg and Arbib, 1998; Jeannerod et al., 1995; Sakata et al., 1995), such a result was expected, but still needed to be established. In LIP, our results confirm the neuronal selectivity documented for position in depth (Genovesio and Ferraina, 2004; Gnadt and Mays, 1995) and for 2D shapes (Lehky and Sereno, 2007; Sereno and Maunsell, 1998), they also fit with the report of 3D orientation-selective neurons in locations that could encompass LIP as defined here (Nakamura et al., 2001). Importantly, we also obtained evidence for the heterogeneous nature

of LIP, with opposing sensitivity gradients for structural and positional stereo information. These gradients foreshadow the sensitivity for structural, but not positional, stereo information in AIP, indicating that AIP and the adjoining portion of LIP are likely to work in close relationship for processing the depth structure of 3D objects. The spatial accuracy required for fine-scale analysis of 3D shape features in these anterior intraparietal regions is in line with the presence of a central visual field representation located in the anterior part of LIP (Ben Hamed et al., 2001; Blatt et al., 1990; Fize et al., 2003).

In CIP, sensitivity to both structural and positional stereo information was revealed using random-line stimuli in line with the joint neuronal encoding of the 3D orientation and 3D position of rod stimuli described for this area (Sakata et al., 1998). At first glance, the weak (if any) sensitivity for small 3D surfaces appears to contradict previous single cell reports (Taira et al., 2000; Tsutsui et al., 2001, 2003). However, our surfaces differed from those employed in these previous studies by the complexity of their contours (generally surfaces with square-shaped outlines have been used in the single cell studies), suggesting that CIP could have a limited role in processing detailed 3D shape features. Our finding that CIP is only sensitive to the contours of large 2D shapes supports this view. This stimulus-size effect fits the observation that neuronal response strength increases monotonically with the size of the stimuli in CIP (Sakata et al., 1999; Shikata et al., 1996), and probably explains why very large stimuli have been used to investigate neuronal properties in this area (Nakamura et al., 2001; Sakata et al., 1998; Tsutsui et al., 2002). Moreover, this size effect can account for the fact that, contrary to the small stereosurfaces used in the second experiment, large stereocheckerboard surfaces efficiently activate CIP (Tsao et al., 2003). In addition, this size effect confirms that stimulus size was the critical difference between the two previous imaging studies concerning the involvement of CIP (pIPS) in 2D shape processing (Denys et al., 2004; Sawamura et al., 2005). Overall, these observations suggest that CIP is more involved in recovering the spatial arrangement of large background elements in the visual scene than in recovering the 3D shape of small objects.

Our finding that both MIP and PIP process stereoscopic information fits with the known involvement of MIP in reaching arm movements (Andersen and Buneo, 2002; Snyder et al., 1997) and with the report (Nakamura et al., 2001) of 3D orientation selective cells in a location encompassing PIP as defined here. Despite their spatial proximity, these areas are functionally segregated by the saccade-related activity found only in MIP (Snyder et al., 2000) and the sensitivity to kinetic depth found only in PIP. Moreover, these areas differ from neighboring area CIP by the absence of 2D shape sensitivity, suggesting that they house representations of the visual scene layout that lack object-related information. Such representations could be sufficient for the control of actions containing guidance and obstacle-avoidance components but no direct interaction with objects, such as arm-reaching movements (Tresilian, 1998).

By showing the prominent role of AIP and anterior LIP in 3D shape processing, our results question the proposal that CIP extracts 3D-shape-related information that is forwarded to AIP for controlling hand manipulation tasks (Sakata et al., 1998, 2005). Sensitivity to 3D shape features emerges in anterior LIP and comes with the uncoupling of structural and positional stereo information, suggesting that salient or behaviorally relevant objects could be isolated from the background in LIP (Gottlieb, 2007; Gottlieb et al., 1998) for analysis of their 3D shape in anterior IPS. It will be the aim of future experiments to test this hypothesis. Also, it will be important to assess whether additional input from ventral visual areas, and in particular the inferotemporal (IT) cortex, which houses neurons selective for complex 2D shapes (Tanaka, 1996), is required to recover fine information about the 3D shape of objects in anterior IPS. Further arguments for such interactions are the selectivity of a distinct group of inferotemporal neurons for the depth structure of the stereo surfaces used in the second experiment (Janssen et al., 1999, 2000) and the direct connections reported between IT and anterior IPS (G. Luppino et al., 2004, Soc. Neurosci., abstract; Webster et al., 1994).

By using the fMRI technique in behaving monkeys, we studied the involvement of parietal areas in processing of stereo information (structural and/or positional) and 3D-shape-related information. This study goes beyond previous imaging studies (Sereno et al., 2002, Tsao et al., 2003, Vanduffel et al., 2002) by demonstrating not only that different parietal areas process distinct aspects of visual 3D space in line with their involvement in distinct sensorimotor functions, but also that 3D shape features are specifically represented in anterior intraparietal regions, where such information is required for the efficient control of hand manipulation tasks.

EXPERIMENTAL PROCEDURES

General Procedures

In total, six male rhesus monkeys (4–7 kg; 4–7 years old) were scanned. Animal care and experimental procedures met the national and European guidelines and were approved by the ethical committee of the K.U. Leuven Medical School. Procedures related to fMRI techniques with behaving monkeys have been described in detail (Fize et al., 2003; Nelissen et al., 2005, 2006; Vanduffel et al., 2001) and are only briefly presented here.

Monkeys sat in a sphinx position within the horizontal bore of the magnet (1.5 T MR scanner Sonata; Siemens), a radial receive-only surface coil positioned above their restrained head. They faced a translucent screen 54 cm from the eyes, and visual stimuli were rear-projected from a Barco 6300 LCD projector. One eye was monitored during scanning using a pupil-corneal reflection tracking system (50 Hz; RK-726PCI, Iscan). A contrast agent (MION, or an equivalent compound, Sinerem) was injected to the animals before each scanning session to improve both contrast-to-noise ratio (Leite et al., 2002; Vanduffel et al., 2001) and spatial selectivity of the MR signal (Mandeville and Marota, 1999; Zhao et al., 2006) compared to BOLD measurements.

Time series were analyzed using SPM99 and MATCH software. Functional volumes (whole brain GE-EPI; TR = 2.4 s; TE = 27 ms; 32 sagittal slices; 8 mm^3 isotropic voxels) were rigidly coregistered with a template anatomy (M12; 0.04 mm^3 isotropic voxels) in stereotaxic space. They were further warped to this template (MATCH algorithm; Chef d'Hotel et al., 2002; Hermosillo et al., 2002; Figure S2A), resliced to 1 mm^3 isotropic voxels, and smoothed with a Gaussian kernel (FWHM = 1.5 mm). Group analyses (fixed effects) were performed with equal number of volumes per monkey, supplemented with single subject analysis. Statistical threshold was set at $p < 10^{-5}$ uncorrected (masked at $p < 10^{-3}$ for overall activation relative to fixation baseline). Realignment and eye movement traces were included as covariates of no interest. Eye movement traces were also analyzed to select the time series and verify that monkeys fixated equally well across the different conditions (Table S1).

Behavioral Tasks

In the stereo test of the first experiment, monkeys (M3, M5, and M11) performed a high-acuity fixation task to prevent disparity-driven vergence eye movements. They interrupted an infrared beam with the hand to signal sudden changes in orientation of a small fixation bar (whose size was set to obtain 80% of correct detections) and received fluid reward for correct responses (Sawamura et al., 2005; Vanduffel et al., 2001).

Monkeys performed a passive fixation task in the motion test of the first experiment (M1, M3, M5, and M11), in the second stereo experiment (M3, M6, and M11), and in the tests with large 2D shapes (M3, M5 and M11) and small 2D shapes (M3 and M5) in the third experiment. They received fluid reward for gazing at a fixation target and maintaining fixation within a small window (±1°, occasionally increased to ± 1.5° vertically to accommodate an artifact caused by the scanning sequence).

In the Saccade test (C. Wardak et al., 2005, Soc. Neurosci., abstract), which was based on a previous study (Koyama et al., 2004), monkeys (M3, M5, and M9) had to saccade toward a red visual target (0.1° × 0.1°) jumping pseudo-randomly among three locations along the horizontal meridian of the screen (0° or ± 7°). To be rewarded, a saccade had to be initiated within 500 ms after target appearance and the fixation held (within a window of about 1° × 2°) until displacement of the visual target to a new position (after about 2.2 s of steady fixation). Mean saccade latency was 350 ms and, on average, a saccade was performed each 2.8 s. In the visual control condition, monkeys had to gaze at a central fixation target (0°) while visual distractors were successively flashed for 350 ms, with 2.2 s intervals, at 7° or 14° of eccentricity either to the left or to the right of the fixation target. Direction and eccentricity of the visual targets in the saccade condition and visual distractors in the visual control condition were balanced (1/2 left and 1/2 right; 2/3 at 7° and 1/3 at 14°).

Experimental Designs

A block design was used in all the experiments. Blocks (conditions) of 10–15 functional volumes immediately succeeding one another were embedded in time series during which 160–225 volumes were acquired. Condition order was pseudorandomized between the time series, but not within a time series (containing 2–4 repetitions of the complete sequence of conditions). All the experiments contained a baseline condition with a fixation spot (0.3° diameter), or a fixation bar in the first stereo experiment (0.2° × 0.05° for M5 and M3 and 0.15° × 0.05° for M11), presented with no visual stimulus in the background. To avoid adaptation during the visual conditions, stimuli were refreshed at a frequency of 0.4 Hz in the stereo and motion tests of the first experiment (new pattern of random lines) at a frequency of 1 Hz in the second experiment (new stereo random-dot surface) and at a frequency of 1.67 Hz in the third experiment (new intact or scrambled 2D shape).

In the first experiment, stimuli (Figures 1A and S4A) were composed of 9 to 12 connected segments forming random angles. They were about 9° in diameter, and the lengths of the segments varied between 0.5° and 9° (width 0.05°). In the stereo test, stimuli were presented binocularly through red/green filter stereoglasses. There were 3 stimuli conditions, with binocular disparity (range of ± 0.6°) specifying 3D structures of random lines (3D structure), 2D patterns outside of the fixation plane (3D position), or without binocular disparity (no disparity). Structural and positional depth sensitivity was assessed by the contrasts 3D structure – 3D position and 3D position – no disparity, respectively. Presentation was monocular in the motion test. There were also three stimuli conditions, with motion specifying rotating 3D structures (3D motion), translating 2D patterns (2D motion), or without motion (static). Sensitivity to kinetic depth specifying 3D structure was revealed by contrasting 3D motion and 2D motion.

In the second experiment, stimuli (Figures 4A and 4B and Figure S4B) consisted of stereo random-dot surfaces embedded in 1 of 4 different 2D shape outlines (Janssen et al., 1999). They measured 5.6° × 5.6° on average, with a dot density of 50% and a dot size of 0.065°, and they were also displayed through red/green filter stereoglasses. Several curvatures (1, 1/2 or 1/4 vertical sinusoidal cycle and antiphase counterparts) and slants (±37° slants about the horizontal, vertical or oblique axes) specified by binocular disparity (range of ± 0.5°) were used for testing 3D curvature and 3D orientation processing in interleaved runs. There were four stimulus conditions in both tests (3D structure, either orientation or curvature in space, 3D position and their respective controls with no disparity). The "no disparity" controls were generated by presenting identical stereo half-images to both eyes (either from the 3D structure or 3D position stimuli). Structural depth sensitivity was assessed by the interaction between 3D information sensitivity and disparity sensitivity, while position in depth processing was targeted by the contrast 3D position – no disparity.

In the third experiment, four stimuli conditions were used for the test with large 2D shapes (~10° on average): intact and scrambled versions of line drawings and grayscale images of objects (Denys et al., 2004; Kourtzi and Kanwisher, 2000). Both the main effect of scrambling and the interaction with image type were assessed. For the small 2D shapes (~5° on average), only grayscale images were used. They were similar to the large grayscale images except that the scrambling grid was removed and the objects (but not the white background) were half-sized. There were four stimulus conditions, corresponding to intact or scrambled versions that were either static or moving. For this study, we targeted 2D shape sensitivity by contrasting the conditions with intact and scrambled versions of the static grayscale images.

Finally, in the Saccade test, saccade-related activity was obtained by contrasting the Saccade and Visual control conditions.

Flattening of the Intraparietal Sulcus

We designed a procedure to flatten the IPS specifically in order (1) to avoid the substantial distortions inherent to the flattening of whole hemispheres or even large cortical regions (Van Essen, 2005), (2) to allow a clear visualization of stereotaxic and anatomical landmarks, and (3) to better control the projection of functional data. A custom-designed algorithm was developed to capture strips of gray matter (Figure S2B) within successive coronal sections of the template anatomy (M12) covering the whole left and right IPS (from y = −18 to +8 mm, in 1 mm steps). These strips were subdivided into adjoining 1 mm segments, whose center was used to derive a flattened representation (Figure S2C) that best preserved the intrinsic 3D geometry of the IPS (with a nonlinear multidimensional scaling; ISOMAP algorithm; Tenenbaum et al., 2000). Voronoi triangulation was then applied to enclose each segment center in the 2D space representation. Thin lines linking segments belonging to the same coronal section indicated antero-posterior levels. The lips and fundus of the IPS were indicated by thick lines passing through the segments corresponding to these anatomical landmarks in each coronal section (gray arrows in Figure S2B).

Statistical scores were assigned to each segment by placing a 2D sampling grid upon their central region (coronal orientation; spacing 0.2 mm; radius 0.3 mm) and computing the median value of the sampled t-scores (calculated by SPM99). Restricting the sampling to the

segments' central region avoided possible contamination between facing segments on the medial and lateral banks of the sulcus. We indicated segments that reached statistical significance by color-coding their corresponding patches on the flat maps.

Path Activity Profiles

Path activity profiles were used to assess (1) the interindividual variability, (2) the magnitude of the effects we observed, and (3) how the activity profiles evolve within, but also between, the activated regions. Symmetrical paths were drawn directly onto the flattened representations of the left and right IPS. Lateral paths run along postero-anterior axes on the IPS lateral banks, passing through CIP, LIP, and AIP, with one segment per coronal level (from −14 to +2 mm). Medial paths run along ventro-dorsal axes on the medial banks, with adjoining coronal segments at y = −11 mm, from the fundus to PIP, and at −10 mm, from MIP to the medial lip.

Time courses of adjusted signal (calculated by SPM99) were extracted from unsmoothed functional volumes (otherwise similar to the smoothed preprocessed volumes) to minimize spatial correlations between neighboring segments. For each segment of these paths, a median time course was computed using the same sampling grid as for the t-score extraction (see previous section). This time course was split into blocks according to the experimental design, and we derived the MR signal for each block by averaging its constituent time points (excluding the first three to take into account the hemodynamic delay). To obtain the mean MR signal change (%) between two conditions, the MR signals associated to the blocks belonging to these two condition were subtracted from each other and averaged (the variability expressed between blocks rather than between successive time points avoid possible temporal correlations between repeated measures).

In plots of the mean MR signal change along the paths (± standard error of the mean), filled symbols indicate data points (flat map segments) with significant sensitivity (i.e. significantly above the 0% difference level) and significant activation (compared to fixation) at the group level and for at least 2/3 of the individuals. Significance was assessed with a one-tailed t test, both at the group level ($p < 0.001$) and for the individual subjects ($p < 0.01$) using only the blocks included in the group analysis. Note that slight differences can arise between the results issued from the analysis of these path activity profiles and those given by SPM99 due to the use of unsmoothed data and additional statistical requirements (significance for 2/3 of the individuals) for the path activity profiles.

In addition, we performed complementary analyses to ensure that the path activation profiles were representative for the regions that were crossed (Figure S2). Paths were enlarged by adding two segments on both sides of each segment initially contained in the paths (Figure S2A). Large paths were thus ~5 mm wide, as opposed to ~1 mm wide for the initial paths. For both the lateral (Figure S2B) and medial (Figure S2C) paths, activity profiles obtained with wider paths were very similar to the ones obtained with the initial paths, arguing in favor of the representativeness of the latter.

Supplemental Data

The Supplemental Data for this article can be found online at http://www.neuron.org/cgi/content/full/55/3/493/DC1/.

ACKNOWLEDGMENTS

The authors are indebted to A. Coeman, C. Fransen, M. Depaep, W. Depuydt, P. Kayenbergh, and G. Meulemens for help with the experiments and to S. Raiguel, R. Vogels, R. Vandenberghe, G. Luppino, M. Imbert, and R. Andersen for comments on earlier versions of the manuscript. The work was supported by grants FWO G151.04, GOA 2005/18, IUAP 5/04, EF/05/014, GSKE, R01 EB000790, EU-projects Insight 2+ and Neurobotics and Fyssen Fundation (J.-B.D). The laboratoire Guerbet (Roissy, France) provided the contrast agent Sinerem.

Received: November 17, 2006
Revised: May 24, 2007
Accepted: June 28, 2007
Published: August 1, 2007

REFERENCES

Andersen, R.A., and Buneo, C.A. (2002). Intentional maps in posterior parietal cortex. Annu. Rev. Neurosci. *25*, 189–220.

Baker, J.T., Patel, G.H., Corbetta, M., and Snyder, L.H. (2006). Distribution of activity across the monkey cerebral cortical surface, thalamus and midbrain during rapid, visually guided saccades. Cereb. Cortex *16*, 447–459.

Ben Hamed, S., Duhamel, J.R., Bremmer, F., and Graf, W. (2001). Representation of the visual field in the lateral intraparietal area of macaque monkeys: A quantitative receptive field analysis. Exp. Brain Res. *140*, 127–144.

Blatt, G.J., Andersen, R.A., and Stoner, G.R. (1990). Visual receptive field organization and cortico-cortical connections of the lateral intraparietal area (area LIP) in the macaque. J. Comp. Neurol. *299*, 421–445.

Boltz, R.L., and Harwerth, R.S. (1979). Fusional vergence ranges of the monkey: A behavioral study. Exp. Brain Res. *37*, 87–91.

Buneo, C.A., and Andersen, R.A. (2006). The posterior parietal cortex: Sensorimotor interface for the planning and online control of visually guided movements. Neuropsychologia *44*, 2594–2606.

Castiello, U. (2005). The neuroscience of grasping. Nat. Rev. Neurosci. *6*, 726–736.

Chef d'Hotel, C., Hermosillo, G., and Faugeras, O. (2002). Flows of diffeomorphisms for multimodal image registration. Proc. IEEE Int. S. Biol. Im. *7–8*, 753–756.

Colby, C.L., and Goldberg, M.E. (1999). Space and attention in parietal cortex. Annu. Rev. Neurosci. *22*, 319–349.

Denys, K., Vanduffel, W., Fize, D., Nelissen, K., Peuskens, H., Van Essen, D., and Orban, G.A. (2004). The processing of visual shape in the cerebral cortex of human and nonhuman primates: A functional magnetic resonance imaging study. J. Neurosci. *24*, 2551–2565.

Fagg, A.H., and Arbib, M.A. (1998). Modeling parietal-premotor interactions in primate control of grasping. Neural Netw. *11*, 1277–1303.

Fize, D., Vanduffel, W., Nelissen, K., Denys, K., Chef d'Hotel, C., Faugeras, O., and Orban, G.A. (2003). The retinotopic organization of primate dorsal V4 and surrounding areas: A functional magnetic resonance imaging study in awake monkeys. J. Neurosci. *23*, 7395–7406.

Gallese, V., Murata, A., Kaseda, M., Niki, N., and Sakata, H. (1994). Deficit of hand preshaping after muscimol injection in monkey parietal cortex. Neuroreport *5*, 1525–1529.

Genovesio, A., and Ferraina, S. (2004). Integration of retinal disparity and fixation-distance related signals toward an egocentric coding of distance in the posterior parietal cortex of primates. J. Neurophysiol. *91*, 2670–2684.

Gnadt, J.W., and Andersen, R.A. (1988). Memory related motor planning activity in posterior parietal cortex of macaque. Exp. Brain Res. *70*, 216–220.

Gnadt, J.W., and Mays, L.E. (1995). Neurons in monkey parietal area LIP are tuned for eye-movement parameters in three-dimensional space. J. Neurophysiol. *73*, 280–297.

Goldberg, M.E., Bisley, J.W., Powell, K.D., and Gottlieb, J. (2006). Saccades, salience and attention: The role of the lateral intraparietal area in visual behavior. Prog. Brain Res. *155*, 157–175.

Goodale, M.A., and Milner, A.D. (1992). Separate visual pathways for perception and action. Trends Neurosci. *15*, 20–25.

Gottlieb, J. (2007). From thought to action: The parietal cortex as a bridge between perception, action, and cognition. Neuron *53*, 9–16.

Gottlieb, J.P., Kusunoki, M., and Goldberg, M.E. (1998). The representation of visual salience in monkey parietal cortex. Nature *391*, 481–484.

Hermosillo, G., Chef d'Hotel, C., and Faugeras, O. (2002). Variational Methods for Multimodal Image Matching. Int. J. Comput. Vis. *50*, 329–343.

Howard, I.P. (2002). Basic Mechanisms, *Volume 1* (Toronto: I. Porteus).

Howard, I.P., and Rogers, B.J. (2002). Depth Perception, *Volume 2* (Toronto: I. Porteus).

Janssen, P., Vogels, R., and Orban, G.A. (1999). Macaque inferior temporal neurons are selective for disparity-defined three-dimensional shapes. Proc. Natl. Acad. Sci. USA *96*, 8217–8222.

Janssen, P., Vogels, R., and Orban, G.A. (2000). Selectivity for 3D shape that reveals distinct areas within macaque inferior temporal cortex. Science *288*, 2054–2056.

Jeannerod, M. (1981). Intersegmental coordination during reaching at natural visual objects. In Attention and Performances IX, J. Long and A. Baddley, eds. (Hillsdale, NJ: Erlbaum), pp. 153–168.

Jeannerod, M. (1986). The formation of finger grip during prehension. A cortically mediated visuomotor pattern. Behav. Brain Res. *19*, 99–116.

Jeannerod, M., Arbib, M.A., Rizzolatti, G., and Sakata, H. (1995). Grasping objects: The cortical mechanisms of visuomotor transformation. Trends Neurosci. *18*, 314–320.

Julesz, B. (1971). Foundations of Cyclopean Perception (Chicago: University of Chicago Press).

Kourtzi, Z., and Kanwisher, N. (2000). Cortical regions involved in perceiving object shape. J. Neurosci. *20*, 3310–3318.

Koyama, M., Hasegawa, I., Osada, T., Adachi, Y., Nakahara, K., and Miyashita, Y. (2004). Functional magnetic resonance imaging of macaque monkeys performing visually guided saccade tasks: Comparison of cortical eye fields with humans. Neuron *41*, 795–807.

Lehky, S.R., and Sereno, A.B. (2007). Comparison of shape encoding in primate dorsal and ventral visual pathways. J. Neurophysiol. *97*, 307–319.

Leite, F.P., Tsao, D., Vanduffel, W., Fize, D., Sasaki, Y., Wald, L.L., Dale, A.M., Kwong, K.K., Orban, G.A., Rosen, B.R., et al. (2002). Repeated fMRI using iron oxide contrast agent in awake, behaving macaques at 3 Tesla. Neuroimage *16*, 283–294.

Lewis, J.W., and Van Essen, D.C. (2000). Mapping of architectonic subdivisions in the macaque monkey, with emphasis on parieto-occipital cortex. J. Comp. Neurol. *428*, 79–111.

Luppino, G., Murata, A., Govoni, P., and Matelli, M. (1999). Largely segregated parietofrontal connections linking rostral intraparietal cortex (areas AIP and VIP) and the ventral premotor cortex (areas F5 and F4). Exp. Brain Res. *128*, 181–187.

Luppino, G., Hamed, S.B., Gamberini, M., Matelli, M., and Galletti, C. (2005). Occipital (V6) and parietal (V6A) areas in the anterior wall of the parieto-occipital sulcus of the macaque: A cytoarchitectonic study. Eur. J. Neurosci. *21*, 3056–3076.

Mandeville, J.B., and Marota, J.J. (1999). Vascular filters of functional MRI: Spatial localization using BOLD and CBV contrast. Magn. Reson. Med. *42*, 591–598.

Melmoth, D.R., and Grant, S. (2006). Advantages of binocular vision for the control of reaching and grasping. Exp. Brain Res. *171*, 371–388.

Murata, A., Gallese, V., Luppino, G., Kaseda, M., and Sakata, H. (2000). Selectivity for the shape, size, and orientation of objects for grasping in neurons of monkey parietal area AIP. J. Neurophysiol. *83*, 2580–2601.

Nakamura, H., Kuroda, T., Wakita, M., Kusunoki, M., Kato, A., Mikami, A., Sakata, H., and Itoh, K. (2001). From three-dimensional space vision to prehensile hand movements: The lateral intraparietal area links the area V3A and the anterior intraparietal area in macaques. J. Neurosci. *21*, 8174–8187.

Napier, J.R. (1980). Hands (London: Geaorge Allen & Unwin Ltd).

Nelissen, K., Luppino, G., Vanduffel, W., Rizzolatti, G., and Orban, G.A. (2005). Observing others: Multiple action representation in the frontal lobe. Science *310*, 332–336.

Nelissen, K., Vanduffel, W., and Orban, G.A. (2006). Charting the lower superior temporal region, a new motion-sensitive region in monkey superior temporal sulcus. J. Neurosci. *26*, 5929–5947.

Orban, G.A., Sunaert, S., Todd, J.T., Van Hecke, P., and Marchal, G. (1999). Human cortical regions involved in extracting depth from motion. Neuron *24*, 929–940.

Orban, G.A., Janssen, P., and Vogels, R. (2006). Extracting 3D structure from disparity. Trends Neurosci. *29*, 466–473.

Rogers, B., and Cagenello, R. (1989). Disparity curvature and the perception of three-dimensional surfaces. Nature *339*, 135–137.

Rozzi, S., Calzavara, R., Belmalih, A., Borra, E., Gregoriou, G.G., Matelli, M., and Luppino, G. (2006). Cortical connections of the inferior parietal cortical convexity of the macaque monkey. Cereb. Cortex *16*, 1389–1417.

Sakata, H., Taira, M., Murata, A., and Mine, S. (1995). Neural mechanisms of visual guidance of hand action in the parietal cortex of the monkey. Cereb. Cortex *5*, 429–438.

Sakata, H., Taira, M., Kusunoki, M., Murata, A., Tanaka, Y., and Tsutsui, K. (1998). Neural coding of 3D features of objects for hand action in the parietal cortex of the monkey. Philos. Trans. R. Soc. Lond. B Biol. Sci. *353*, 1363–1373.

Sakata, H., Taira, M., Kusunoki, M., Murata, A., Tsutsui, K., Tanaka, Y., Shein, W.N., and Miyashita, Y. (1999). Neural representation of three-dimensional features of manipulation objects with stereopsis. Exp. Brain Res. *128*, 160–169.

Sakata, H., Tsutsui, K., and Taira, M. (2005). Toward an understanding of the neural processing for 3D shape perception. Neuropsychologia *43*, 151–161.

Sawamura, H., Georgieva, S., Vogels, R., Vanduffel, W., and Orban, G.A. (2005). Using functional magnetic resonance imaging to assess adaptation and size invariance of shape processing by humans and monkeys. J. Neurosci. *25*, 4294–4306.

Sereno, A.B., and Maunsell, J.H. (1998). Shape selectivity in primate lateral intraparietal cortex. Nature *395*, 500–503.

Sereno, M.E., Trinath, T., Augath, M., and Logothetis, N.K. (2002). Three-dimensional shape representation in monkey cortex. Neuron *33*, 635–652.

Servos, P., Goodale, M.A., and Jakobson, L.S. (1992). The role of binocular vision in prehension: A kinematic analysis. Vision Res. *32*, 1513–1521.

Shikata, E., Tanaka, Y., Nakamura, H., Taira, M., and Sakata, H. (1996). Selectivity of the parietal visual neurones in 3D orientation of surface of stereoscopic stimuli. Neuroreport *7*, 2389–2394.

Smeets, J.B., and Brenner, E. (1999). A new view on grasping. Motor Control *3*, 237–271.

Snyder, L.H., Batista, A.P., and Andersen, R.A. (1997). Coding of intention in the posterior parietal cortex. Nature *386*, 167–170.

Snyder, L.H., Batista, A.P., and Andersen, R.A. (2000). Saccade-related activity in the parietal reach region. J. Neurophysiol. *83*, 1099–1102.

Taira, M., Mine, S., Georgopoulos, A.P., Murata, A., and Sakata, H. (1990). Parietal cortex neurons of the monkey related to the visual guidance of hand movement. Exp. Brain Res. *83*, 29–36.

Taira, M., Tsutsui, K.I., Jiang, M., Yara, K., and Sakata, H. (2000). Parietal neurons represent surface orientation from the gradient of binocular disparity. J. Neurophysiol. *83*, 3140–3146.

Tanaka, K. (1996). Inferotemporal cortex and object vision. Annu. Rev. Neurosci. *19*, 109–139.

Tenenbaum, J.B., de Silva, V., and Langford, J.C. (2000). A global geometric framework for nonlinear dimensionality reduction. Science *290*, 2319–2323.

Tresilian, J.R. (1998). Attention in action or obstruction of movement? A kinematic analysis of avoidance behavior in prehension. Exp. Brain Res. *120*, 352–368.

Tsao, D.Y., Vanduffel, W., Sasaki, Y., Fize, D., Knutsen, T.A., Mandeville, J.B., Wald, L.L., Dale, A.M., Rosen, B.R., Van Essen, D.C., et al. (2003). Stereopsis activates V3A and caudal intraparietal areas in macaques and humans. Neuron *39*, 555–568.

Tsutsui, K., Jiang, M., Yara, K., Sakata, H., and Taira, M. (2001). Integration of perspective and disparity cues in surface-orientation-selective neurons of area CIP. J. Neurophysiol. *86*, 2856–2867.

Tsutsui, K., Sakata, H., Naganuma, T., and Taira, M. (2002). Neural correlates for perception of 3D surface orientation from texture gradient. Science *298*, 409–412.

Tsutsui, K., Taira, M., and Sakata, H. (2005). Neural mechanisms of three-dimensional vision. Neurosci. Res. *51*, 221–229.

Ungerleider, L.G., and Mishkin, M. (1982). Two cortical visual systems. In Analysis of Visual Behavior, D.J. Ingle, M.A. Goodale, and R.J. Mansfield, eds. (Cambridge, MA: MIT Press), pp. 549–586.

Van Essen, D.C. (2005). A Population-Average, Landmark- and Surface-based (PALS) atlas of human cerebral cortex. Neuroimage *28*, 635–662.

Vanduffel, W., Fize, D., Mandeville, J.B., Nelissen, K., Van Hecke, P., Rosen, B.R., Tootell, R.B., and Orban, G.A. (2001). Visual motion processing investigated using contrast agent-enhanced fMRI in awake behaving monkeys. Neuron *32*, 565–577.

Vanduffel, W., Fize, D., Peuskens, H., Denys, K., Sunaert, S., Todd, J.T., and Orban, G.A. (2002). Extracting 3D from motion: Differences in human and monkey intraparietal cortex. Science *298*, 413–415.

Wallach, H., and O'Connell, D.N. (1953). The kinetic depth effect. J. Exp. Psychol. *45*, 205–217.

Watt, S.J., and Bradshaw, M.F. (2003). The visual control of reaching and grasping: Binocular disparity and motion parallax. J. Exp. Psychol. Hum. Percept. Perform. *29*, 404–415.

Webster, M.J., Bachevalier, J., and Ungerleider, L.G. (1994). Connections of inferior temporal areas TEO and TE with parietal and frontal cortex in macaque monkeys. Cereb. Cortex *4*, 470–483.

Wheatstone, C. (1838). Contribution to the physiology of vision - Part the first On some remarkable and hitherto unobserved phenomena of binocular vision. Philos. Trans. R. Soc. Lond. B Biol. Sci. *128*, 371–394.

Zhao, F., Wang, P., Hendrich, K., Ugurbil, K., and Kim, S.G. (2006). Cortical layer-dependent BOLD and CBV responses measured by spin-echo and gradient-echo fMRI: Insights into hemodynamic regulation. Neuroimage *30*, 1149–1160.